Atmos. Chem. Phys. Discuss., 11, 2473–2501, 2011
www.atmos-chem-phys-discuss.net/11/2473/2011/
doi:10.5194/acpd-11-2473-2011

Atmospheric Chemistry and Physics Discussions

The effects of a solar eclipse on photo-oxidants in different areas of China

J.-B. Wu[1,5], Z. F. Wang[1], W. Zhang[2], H. B. Dong[1], X. L. Pan[1], C.-Y. Lin[3], and P. H. Xie[4]

[1]State Key Laboratory of Atmospheric Boundary Layer Physics and Atmospheric Chemistry (LAPC), Institute of Atmospheric Physics, Chinese Academy of Science, Beijing 100029, China
[2]Aviation Meteorological Center of China, Beijing 100122, China
[3]Research Center for Environmental Changes, Academia Sinica, Taipei, Taiwan
[4]Key Lab. Of Environment Optics & Technology, Anhui Institute of Optics and Fine Mechanics, Chinese Academy of Sciences, Hefei, China
[5]Graduate University of Chinese Academy of Science, Beijing, China

Received: 31 December 2010 – Accepted: 15 January 2011 – Published: 24 January 2011

Correspondence to: Z. F. Wang (zifawang@mail.iap.ac.cn)

Published by Copernicus Publications on behalf of the European Geosciences Union.

Abstract

This study investigates the effects of the total solar eclipse of 22 July 2009 on surface ozone and other photo-oxidants over central China using the WRF-Chem model. Chemical and meteorological observation data were used to validate the model, and results suggest that the WRF-Chem model can capture the effects of the total solar eclipse well. The maximum impacts of the eclipse occur over the area of totality, with a decrease in surface temperature of 1.5 °C and decrease in wind speed of 1 m s^{-1}. In contrast, the maximum impacts on atmospheric pollutants occur over parts of north and east China where emissions are greater, with an increase of 5 ppbv in NO_2 and 25 ppbv in CO and a decrease of 10 ppbv in O_3 and 3 ppbv in NO. This study also shows the effects of the solar eclipse on surface photo-oxidants in different parts of China. Although the sun was obscured to a smaller extent in polluted areas than in clean areas, the impacts of the eclipse in polluted areas are greater and last longer than they do in clean areas. The change in radical concentrations during the eclipse reveals that nighttime chemistry dominates in both polluted and clean areas. In contrast to the effects on atmospheric pollutants, the change in radical concentrations (OH, HO_2 and NO_3 in clean areas is much larger than in polluted areas mainly because of the limited sources of radicals in these areas. In addition, since solar eclipse does provide a natural opportunity to test our understanding more thoroughly on atmospheric chemistry, especially on photolysis-related chemistry, a comprehensive experimental campaign is highly recommended during solar eclipses in future.

1 Introduction

Solar eclipse provides a rare opportunity as well as a challenge to investigate how meteorological and photochemical processes respond to relatively abrupt change of the incident solar radiation.

ACPD
11, 2473–2501, 2011

Temperature, solar irradiation, relative humidity, wind and cloudiness within the surface layer are among the most common meteorological parameters explored by several studies during solar eclipses (Fernandez et al., 1993, 1996; Hanna, 2000; Psiloglou and Kambezidis, 2007; Amiridis et al., 2007; Emde et al., 2007; Kazadzis et al., 2007). The drop in surface temperature during a solar eclipse is of broad interest and becomes noticeable when the sun is about half-covered (Anderson, 1999). In general, the results of most studies indicate the similar patterns of temperature changes with the lowest values occurring a few minutes after the full phase, but the precise reduction may not directly determined by eclipse magnitude, but by surrounding environment and local conditions (Founda et al., 2007; Gerasopoulos et al., 2008). Recent researches into the meteorological effects of solar eclipses reveal a decrease in the mean wind speed during the eclipse, and this is attributed to the combined effect of a decrease in the thermal gradient and the stabilization of the surface layer due to the temperature drop (Amiridis et al., 2007).

Solar eclipses also enable the evaluation of the response of the gas-phase chemistry of photo-oxidants during a drastic perturbation in solar radiation. Plausible variations in stratospheric composition caused by solar eclipses have been addressed by some studies (Mims and Mims, 1993; Zerefos et al., 2000; Gogosheva et al., 2002; Gerasopoulos et al., 2008). However, there are only a limited number of studies focusing on the effects on tropospheric ozone and other photo-oxidants. A decrease of around 10–15 ppbv in surface ozone concentration was observed at Thessaloniki, Greece, during the solar eclipse of 11 August 1999, with a lag-time between the maximum of the eclipse and the maximum of the induced ozone decrease (Zerefos et al., 2001; Tzanis, 2005). Both measurements and model simulations in this event have shown that the partitioning of NO_x between NO and NO_2 is determined almost exclusively by variations in JNO_2 (Fabian et al., 2001). In the total solar eclipse of 29 March 2006, observations and modeling show that there is a significant decrease in O_3 and NO and an increase in NO_2 at polluted sites, while there is no clear impact on these pollutants at the unpolluted sites (Zanis et al., 2007). The decrease in the surface ozone concentration

ACPD
11, 2473–2501, 2011

that observed after the beginning of the eclipse lasted two hours, probably due to the decreased efficiency of the photochemical ozone formation (Tzanis et al., 2008).

Although the most important chemical mechanisms affecting atmospheric composition have been identified and studied, further investigation is necessary to explain the complex interactions involving meteorological, topographic, emission and chemical parameters (Varotsos, 1994, 2005). In addition, solar eclipses are unique since they happen in different seasons, at different times of day, in different locations and under different synoptic conditions. On 22 July 2009 a total solar eclipse was visible along a narrow band across China from western Asia to the Pacific Ocean (Fig. 1b), while a partial eclipse was seen within a much broader area along the main axis. After leaving mainland Asia, the path curves southeastward across the Pacific Ocean. A partial eclipse is seen within the much broader path of the Moon's penumbral shadow, and this covers most of eastern Asia, and the Pacific Ocean. More details on the path of the eclipse and particular local circumstances can be found at the eclipse web site of NASA (http://eclipse.gsfc.nasa.gov/SEmono/TSE2009/TSE2009.html). This solar eclipse's umbral shadow first touched down in China at 00:56 UTC and left the mainland at 03:04 UTC, more than 2-hour occurring in China which may have a significant impact on atmospheric composition. And this provides a natural perturbation to atmospheric chemistry that allows us to test our understanding more thoroughly.

The present study investigates the chemical changes occurring during the total solar eclipse of 22 July 2009, focusing on surface ozone and other photo-oxidants in different parts of China. In order to simulate the changes in both meteorological and chemical variables during the eclipse, an online numerical approach was adopted using the WRF-Chem model. A full description of the method and validation of experiments is given in Sect. 2; Sect. 3 describes the main results of the experiments and the conclusions are presented in Sect. 3.

ACPD
11, 2473–2501, 2011

2 The description and validation of model

2.1 Method

Numerical simulations were carried out using the WRF-Chem model, version 3.1.1. The WRF-Chem model is a newly developed regional chemical/transport model coupled online with the Weather Research and Forecasting (WRF) model. The WRF model is a new generation meso-scale numerical weather prediction system designed to serve both operational forecasting and atmospheric research needs. It is a fully compressible and non-hydrostatic model and a detailed description can be found on the WRF model website (http://www.wrf-model.org). The Chem model is fully consistent with the WRF model, with the same vertical and horizontal coordinates, time step, transport scheme, and physical parameterization schemes. A detailed description of WRF-Chem is given by Grell et al. (2005) and Fast et al. (2006), and more information can be found at the website (http://ruc.noaa.gov/wrf/WG11/).

The WRF-Chem model used in this study has a vertical structure consisting of 27 σ-levels extending from 1000 to 50 hPa. The following model parameterizations have been chosen to simulate atmospheric conditions:

- The Rapid Radiative Transfer Model – RRTM (Mlawer, 1997) scheme was used as the solver for long wave radiation and the Dudhia scheme (Dudhia, 1989) for the short wave. In these studies the radiation modules were called every minute to account for the parameterization of the eclipse which was inserted into this module,
- the Mellor-Yamada-Janjic TKE scheme for turbulence in the PBL and in the free atmosphere (Janjic, 1994),
- the Lin microphysics scheme was used in order to simulate atmospheric microphysics,

ACPD
11, 2473–2501, 2011

– the CBMZ chemical mechanism (Zaveri et al., 1999; Fast et al., 2006) with MOSAIC aerosol module (Zaveri et al., 2008) were used to simulate the chemical conditions,

– the Fast-J photolysis scheme (Wild et al., 2000; Barnard et al., 2004; Fast et al., 2006) was used to calculate photolysis rates during the solar eclipse, and the module was called every minute for consistency with the radiation schemes.

There are two major obstacles in reproducing the solar eclipse phenomenon and its effects on the atmosphere using a numerical model:

1. Inserting the eclipse path (including total and partial eclipse) into the model, and following its progression over the Earth during the day.

2. Calculating the precise percentage obscuration during the eclipse corresponding to the latitude and longitude of each grid point in the simulation domain every time-step (Fig. 1b).

The problem of reproducing the solar eclipse was solved by varying the solar constant and photolysis rates to the same extent at a given time. The variations were introduced by the use of a scaling factor dependent on latitude, longitude and time which was proportional to the distance from the center of the total eclipse and which moved with a specified velocity. The radiation scheme and photolysis scheme were both called every minute, and the distance of each grid point to the center of the total eclipse was calculated with a unified formula referred to the path of the umbral shadow observed by NASA (http://eclipse.gsfc.nasa.gov/SEmono/TSE2009/TSE2009tab/TSE2009-Table03.pdf). The solar constant and photolysis rates during the eclipse event (00:55–04:15 UTC) were scaled by this factor as a function of latitude, longitude and time.

In order to investigate the effects of the solar eclipse on meteorological and chemical parameters, the WRF-Chem modeling system was run twice, once with the moving umbra of the Moon (Eclipse), and once without it (NoEclipse).

ACPD
11, 2473–2501, 2011

2.2 Validation experiment

The observation sites are showed in Fig. 1a, with yellow points representing the sites of downward solar radiation data, blue points representing the sites of 2-m temperature, and red points representing the sites of atmospheric pollutants. The downward solar radiation data is obtained from SKYNET (http://atmos.cr.chiba-u.ac.jp/). The surface air temperature data is collected from observation in the airports, with 1 min time resolution. And the atmospheric pollutants (O_3 and NO_2) data is attained from the local measurement in Hefei and Tongcheng, with 5 min time resolution. According to the satellite image (Fig. 1a), several sites such as Wuhan (WH), Tongcheng (TC), Hefei (HF), Hedo and Fukue are somewhat influenced by light cloud. However, there is no rain during the solar eclipse period according to the local observation. Therefore the observation data is valid for comparison with WRF-Chem simulation.

2.2.1 Downward solar radiation

The immediate effect of the solar eclipse is on solar radiation. It is well known that the variation in the downward solar radiation is approximately proportional to the obscuration of the sun. The temporal variation of the downward solar radiation (Fig. 2) show a sharp decrease at Hedo and Fukue in both the observations and the Eclipse run, while in the NoEclipse run no reduction in radiation is seen. Clearly the Eclipse run is capable of reproducing the downward solar radiation well when compared to measured data.

2.2.2 Temperature at 2-m

The time series of observed and simulated 2-m temperature at different sites during the eclipse hours are shown in Fig. 3. Chongqing and Wuhan (Fig. 3c and d) lie in the path of the total solar eclipse, while other sites experienced a partial solar eclipse, with Beijing and Shenyang, (Fig. 3a and b) lying approximately 10 degrees to the north

ACPD
11, 2473–2501, 2011

and Guangzhou and Shenzhen (Fig. 3e and f) lying 7 degrees to the south. The double arrow denotes the maximum eclipse and the maximum difference in temperature between the Eclipse and NoEclipse runs. The temperature drop followed a similar and obvious pattern in both observations and the Eclipse run at all stations as evident from Fig. 3, while in the NoEclipse run the temperature generally increased without any drop. Apart from the amplitude of the temperature drop, the timing of the simulated response is also consistent with the observations. Besides, the time of the minimum temperature occurrence at these sites is very close to the full phase of the solar eclipse. However, the amplitudes of the temperature change are different at each location. The maximum difference in temperature between the Eclipse and NoEclipse run is 2.12 °C and 2.03 °C in Chongqing and Wuhan (under the total eclipse) respectively, larger than that in stations with the partial eclipse. This is largely related to the different percentage of obscuration. Generally, the results of the Eclipse run agree quite well with measured data during the solar eclipse.

2.2.3 NO_2 and O_3

The performance of the Eclipse experiment for atmospheric pollutants is demonstrated for surface O_3 and NO_2 at Hefei and Tongcheng, which are located in the path of the total eclipse and are characterized by different air pollution levels. The observation showed that during the eclipse hours, the surface ozone displayed a decrease of around 20 ppbv in Hefei, while at the relatively unpolluted site of Tongcheng the surface ozone showed a decrease of 5–10 ppbv. The measured NO_2 showed an increase of at most 10 and 3 ppbv in Hefei and Tongcheng respectively. Both measurement and model simulation in the Eclipse experiment showed a very similar pattern in surface O_3 and NO_2, while the NoEclipse run showed steady increases or decreases typical of normal conditions. At the relatively unpolluted site of Tongcheng, the Eclipse run matched very well with observations both in magnitude and pattern. At the polluted site of Hefei, the Eclipse run paralleled the measurements but was offset to lower concentrations. This bias may be related to the coarse resolution of the model, which

ACPD
11, 2473–2501, 2011

may underestimate emissions at polluted sites. However, the Eclipse run can mostly simulate the basic features of atmospheric pollutants during the solar eclipse.

In conclusion, based on the comparison between model simulations and measurements above, the Eclipse experiment captures the main characteristics of the solar eclipse and its effects on atmospheric composition.

3 Results of experiments

3.1 Total effects of the solar eclipse

The effects of the solar eclipse over China as calculated by WRF-Chem are depicted in Fig. 5 which shows the difference in 2-m temperature, surface wind speed, NO_2, CO, O_3, and NO between Eclipse and NoEclipse conditions for the lowest model level averaged over the time window 01:00–02:00 UTC.

The simulated temperature response (Fig. 5a) is distinct mainly over mainland China with more pronounced anomalies (about −1.5 °C) over the eclipse's totality areas (central China), while the effect of the eclipse is minimized by the sea due to its thermodynamics character. And there an addition zone with low differences between north and central China. This low-difference zone resulted from cloud coverage, which greatly reduces the impact of the solar eclipse. The location of this zone is consistent with cloud cover in the satellite image (Fig. 1a), which suggests that the simulation of the solar eclipse is reasonable. It can be concluded that the magnitude of surface air temperature is not just depended on the sun obscuration induced by eclipse but on a combination of several factors such as sun obscuration, vegetation and local cloudiness.

The simulated wind speed response (Fig. 5b) shows a similar pattern as temperature does, with a decrease of approximately 1 m s^{-1} over the eclipse totality area. It is worth-noting that the wind speed drop is noticeable when the air temperature over the same area decreases more than 1 °C. This can be resulted from combined effect of a

ACPD
11, 2473–2501, 2011

decrease in the thermal gradient and the stabilization of the surface layer induced by the temperature drop.

In contrast to the meteorological variables, the impacts of the solar eclipse on atmospheric pollutants (Fig. 5c–f) are greatest over parts of north and east China where the maximum emissions occur. We find an increase of 5 ppbv in NO_2 and 25 ppbv in CO, and a decrease of 10 ppbv in O_3 and 3 ppbv in NO. Solar radiation changes during an eclipse may affect tropospheric photo-oxidants in several ways on different timescales. A perturbation to the photo-stationary steady state of O_3, NO and NO_2 is induced immediately during a solar eclipse through Reactions (R1), (R2) and (R3):

$$NO_2 + h\nu \ (\lambda < 424 \text{ nm}) \rightarrow O(^3P) + NO \quad \text{(R1)}$$

$$O(^3P) + O_2 + M \rightarrow O_3 + M \quad \text{(R2)}$$

$$NO + O_3 \rightarrow NO_2 + O_2 \quad \text{(R3)}$$

As a direct consequence the primary pollutant NO destroys O_3 through the titration Reaction (R3) without O_3 being reformed through NO_2 photolysis (R1). Therefore, the photo-stationary steady state of O_3, NO and NO_2 is expected to be very susceptible to solar radiation change during the solar eclipse event, as be well described in Fig. 5c–e. The increase of CO may be related to dynamic process, discussed below.

During the eclipse hours, it can be concluded that the solar eclipse has clear impacts on atmospheric pollutants over high-emission areas and on the meteorological variables around the areas of totality.

3.2 Effects in different areas

The results discussed in the previous sections indicate that the effects of the solar eclipse are significant. In particular, since the results of experiments Eclipse and NoEclipse suggest that the eclipse can have a greater impact on atmospheric pollutants in areas with higher emissions even though solar obscuration is less, there is strong

ACPD
11, 2473–2501, 2011

motivation to investigate the effects of the eclipse in different areas further. For this purpose, we focus on surface photo-oxidants in two areas with different emission levels (Fig. 1b). The area in north China, referred to here as the "polluted area", has a higher emission level than the area (termed the "clean area") in central China. Furthermore, the maximum solar obscuration is different in these two areas, averaging 74.1% in the polluted area and 96.8% in the clean area. These two areas are little affected by cloud (demonstrated by the satellite image, Fig. 1a) which could greatly reduce the effect of the eclipse. Based on the distinct characteristics in these two areas, we can gain a clear understanding of the effects of the eclipse.

The average differences in O_3, NO_2 and NO between Eclipse and NoEclipse conditions in the WRF-Chem simulations over the time window of the eclipse (00:00–05:00 UTC) are given in Table 1. In the polluted area, the WRF-Chem simulations indicate an ozone decrease of 5.2 ppbv, almost twice than of the clean area. Similarly the WRF-Chem simulations indicate small changes in NO and NO_2 in the clean area during the solar eclipse. In particular, the increase in NO_2 of 3.2 ppbv and the decrease in NO of 1.5 ppbv have been calculated at the time of maximum solar coverage in the polluted area. The net effect of O_3, NO_2 and NO can be attributed to the perturbation of the photostationary state of O_3, NO_2 and NO during the eclipse, with NO_2 generated from the titration reaction of O_3 with NO and not being efficiently photolysed. In the solar eclipse over China, the response of O_3, NO_2 and NO in the polluted area is much larger than those in the clean area. In addition, it is found that there is an increase in CO of 10.6 ppbv in the polluted area but only a small change in the clean area.

The altitude-time cross sections of the effects of the eclipse on O_3, NO_2, and NO in the polluted and clean areas are shown in Fig. 6. These show that:

– In the polluted area, the maximum responses of O_3, NO_2 and NO induced by solar eclipse are of the order of 10 ppbv, 3 ppbv and −1.5 ppbv respectively, while the corresponding values in clean area are much smaller. Although the maximum

ACPD
11, 2473–2501, 2011

solar obscuration is smaller in the polluted area than in clean area, the impacts of the eclipse in the polluted area are greater in magnitude, and last longer than those in the clean area.

- It is worth noting that there is an increase in NO after the initial sharp decrease at the beginning of solar eclipse. Since the NO_2 can be accumulated during the solar eclipse (see Fig. 6b), the photolysis of the accumulated NO_2 once the solar radiation is recovering could generate extra NO, and hence result in sharp increase of NO after eclipse even during the partial eclipse period when solar radiation reappears.

- The effect of the eclipse on atmospheric pollutants is mainly within the planetary boundary layer (below 1500 m). This is important because a majority of atmospheric pollutants remain in the planetary boundary layer.

It is interesting to find that there is reduced CO right above the enhanced layer of surface CO (Fig. 7), with almost the same magnitude of CO concentrations in these two regions. This is contributed to the downward flow below 1500 m which is caused by temperature drop during the solar eclipse event. The downward flow may bring pollutants down to the surface, resulting in an increase in concentration at the surface and decrease in the layer above in both polluted and clean areas. Although the change in CO in the clean area shows a very similar pattern as in the polluted area, but the magnitude of anomaly CO concentration is much smaller in the clean area because of the lower emission rate. Since the chemical lifetime of CO is relatively long, the changes in CO near the surface are mainly attributed to vertical transport induced by the dynamic disturbance during the solar eclipse event.

The WRF-Chem model simulates a sharp change from daytime to nighttime chemistry as depicted in Fig. 8. During the eclipse period hydroxyl (OH) and hydrogen peroxy (HO_2) radicals, mainly photo-chemically produced, show rapid decrease by more than an order of magnitude to nighttime levels. Simultaneously the model simulations show that the nitrate (NO_3) radical – mainly present during the night – increases during the

ACPD
11, 2473–2501, 2011

eclipse hours. Reactive radicals involved in atmospheric chemistry are strongly dependent on the photolysis rate constant JO^1D for photo-dissociation of ozone in the near UV (R4, R5) and the photolysis of HCHO (R6). During the solar eclipse when nighttime chemistry dominates, an additional source of radicals occurs through reaction of alkenes and ozone (R7). These reactions together induce changes in OH and HO_2 concentrations which in turn bring changes in the rates of ozone loss via Reactions (R8) and (R9).

$$O_3 + h\nu\ (\lambda < 320\ \text{nm}) \rightarrow O^1D + O_2 \quad \text{(R4)}$$

$$O^1D + H_2O \rightarrow OH \quad \text{(R5)}$$

$$HCHO + h\nu \rightarrow 2HO_2 \quad \text{(R6)}$$

$$\text{Alkene} + O_3 \rightarrow \text{radicals} \quad \text{(R7)}$$

$$HO_2 + O_3 \rightarrow OH + 2O_2 \quad \text{(R8)}$$

$$OH + O_3 \rightarrow HO_2 + O_2 \quad \text{(R9)}$$

It is worth noting that the change of these three radicals in polluted areas is smaller than in clean areas, which is opposite of the changes seen for atmospheric pollutants. In the clean area, the radicals come from the photolysis of O_3 through Reactions (R4) and (R5), and the yield from this reaction is rather small during the solar eclipse which results in a sharp change in radicals. In contrast, the source of radicals in the polluted area is diverse through Reactions (R4), (R5), (R6) and (R7), and as a result, the change in radicals is smaller. In addition, although the change in radical concentrations in the clean area is larger during the solar eclipse period, the difference becomes negligible soon after the eclipse. In the polluted area however, the effect of the eclipse on radical concentrations is still clear after eclipse. The impact of solar eclipse in the polluted area lasts longer than in the clean area, which is consistent with the finding discussed above.

ACPD
11, 2473–2501, 2011

The average impact of the solar eclipse on photo-oxidants in different areas is shown in Table 2. The impact of the solar eclipse is calculated using the formula: Percentage = (Eclipse – NoEclipse)/NoEclipse × 100%. We calculate the average impact in three stages according to the development of solar eclipse (solar obscuration >50%, <50% and 2 h after the eclipse). The effect of the eclipse on ozone is larger in the polluted area, with a difference of −7% compared to the clean area in the whole eclipse period. NO_x is more sensitive to the eclipse, with an impact of up to 50% during the obscuration period (>50%) in both areas. The variation in solar radiation during the eclipse results in rapid changes in radicals (OH, HO_2, NO_3), especially during obscuration (>50%), and the impact in the clean area can be up to 60% which is largely because of the single source of radicals in this area. As the solar radiation recovers, the concentrations of radicals in the clean area return to normal rapidly. However in the polluted area, the impact on the radicals lasts longer, mainly because of the multiple sources of radicals in this area. In conclusion, the effect of the eclipse at its peak is significant in both areas, but the effects last longer in polluted areas.

4 Summary and discussions

This study investigates the effects on surface ozone and other photo-oxidants of the total solar eclipse of 22 July 2009, focusing on different regions in China. In order to study the effects of the eclipse on meteorological and chemical parameters, the WRF-Chem modeling system was run twice, once with the moving umbra of the Moon, and once without it. The WRF-Chem model captures the basic features of the total solar eclipse well.

The solar eclipse has maximum impact in the region of totality, with a decrease in surface temperature of 1.5 °C and decrease in wind speed of 1 m s^{-1}. In contrast to the meteorological variables, the maximum impacts on atmospheric pollutants occur over areas of north and east China where emissions are greater, with an increase of 5 ppbv in NO_2 and 25 ppbv in CO and a decrease of 10 ppbv in O_3 and 3 ppbv in NO.

ACPD
11, 2473–2501, 2011

Furthermore, this study shows the effects of the solar eclipse on surface photo-oxidants in different parts of China. Although the sun was obscured to a smaller extent in polluted areas than in clean areas, the impacts of the eclipse in polluted areas are larger and last longer than those in clean areas. It is worth noting that there is an increase in NO following the sharp decrease which occurs during the maximum in the eclipse, and this may be related to NO_2 photolysis, which leads to accumulation of NO as solar radiation recovers. The results also show that the changes in CO around the surface are mainly due to dynamic processes. The change of radical concentrations during the eclipse reveals that nighttime chemistry dominates in both polluted and clean areas. However, in contrast to the change in atmospheric pollutants, the change in radical concentrations (OH, HO_2 and NO_3) in clean areas is much greater than that in polluted areas mainly because of the limited source of radicals in these areas.

It is a pity that a comprehensive experimental campaign is not organized during the total solar eclipse of 22 July 2009. And it should be pointed out that the 2-site measurement of atmospheric pollutants used in this study is somewhat not enough. Therefore, we conduct a numerical approach using an online model WRF-Chem to investigate the impact of the total solar eclipse, and reproduce the basic features of this solar eclipse. However, it is better that more observation data of atmospheric pollutants could be analyzed or used as validation of numerical model. As mentioned in this study above, solar eclipse does provide a natural perturbation to atmospheric chemistry that allows us to test our understanding more thoroughly. Thus a comprehensive experimental campaign is highly recommended during the solar eclipses in future. And the specific preparation for these measurements is quite capable because these are, after all, highly predictable events. More importantly, the high time resolution measurements of atmospheric compositions are recommended here: (i) ozone (O_3), nitrogen oxides (NO and NO_2), (ii) photolysis rates that can be observed, (iii) hydroxyl (OH), hydrogen peroxy (HO_2) and nitrate (NO_3) radicals that have drastic changes from daytime to nighttime chemistry, (iv) VOCs that is sensitive to solar radiation, (v) some photolysis-related atmospheric compositions that have unknown sources, such as HONO.

ACPD
11, 2473–2501, 2011

Acknowledgement. This study is funded by the Chinese Academy of Science (KZCX2-YW-205) and NSFC (40775077). The authors gratefully thank Professor Oliver Wild in the Lancaster University of UK for pre-viewing.

References

Abram, J. P., Creasey, D. J., Heard, D. E., Lee, J. D., and Pilling, M. J.: Hydroxyl radical and ozone measurements in England during the solar eclipse of 11 August 1999, Geophys. Res. Lett., 27, 3437–3440, 2000.

Amiridis, V., Melas, D., Balis, D. S., Papayannis, A., Founda, D., Katragkou, E., Giannakaki, E., Mamouri, R. E., Gerasopoulos, E., and Zerefos, C.: Aerosol Lidar observations and model calculations of the Planetary Boundary Layer evolution over Greece, during the March 2006 Total Solar Eclipse, Atmos. Chem. Phys., 7, 6181–6189, doi:10.5194/acp-7-6181-2007, 2007.

Anderson, J.: Meteorological changes during a solar eclipse, Weather, 54(7), 207–215, 1999.

Barnard, J. C., Chapman, E. G., Fast, J. D., Schmelzer, J. R., Slusser, J. R., and Shetter, R. E.: An evaluation of the FAST-J photolysis algorithm for predicting nitrogen dioxide photolysis rates under clear and cloudy sky conditions, Atmos. Environ., 38, 3393–3403, doi:10.1016/j.atmosenv.2004.03.034, 2004.

Dudhia, J.: Numerical Study of Convection Observed during the Winter Monsoon Experiment Using a Mesoscale Two-Dimensional Model, J. Atmos. Sci., 46, 3077–3107, 1989.

Emde, C. and Mayer, B.: Simulation of solar radiation during a total eclipse: a challenge for radiative transfer, Atmos. Chem. Phys., 7, 2259–2270, doi:10.5194/acp-7-2259-2007, 2007.

Fabian, P., Rappengluck, B., Stohl, A., Werner, H., Winterhalter, M., Schlager, H., Stock, P., Berresheim, H., Kaminski, U., Koepke, P., Reuder, J., and Birmili, W.: Boundary layer photochemistry during a total solar eclipse, Meteorol. Z., 10, 187–192, 2001.

Fast, J. D., Gustafson, W. I., Easter, R. C., Zaveri, R. A., Barnard, J. C., Chapman, E. G., Grell, G. A., and Peckham, S. E.: Evolution of ozone, particulates, and aerosol direct radiative forcing in the vicinity of Houston using a fully coupled meteorology-chemistry-aerosol model, J. Geophys. Res., 111, D21305, doi:10.1029/2005jd006721, 2006.

Fernandez, W., Castro, V., and Hidalgo, H.: Air-Temperature and Wind Changes in Costa-Rica during the Total Solar Eclipse of 11 July 1991, Earth Moon Planets, 63, 133–147, 1993.

ACPD

11, 2473–2501, 2011

Fernandez, W., Hidalgo, H., Coronel, G., and Morales, E.: Changes in meteorological variables in Coronel Oviedo, Paraguay, during the total solar eclipse of 3 November 1994, Earth Moon Planets, 74, 49–59, 1996.

Founda, D., Melas, D., Lykoudis, S., Lisaridis, I., Gerasopoulos, E., Kouvarakis, G., Petrakis, M., and Zerefos, C.: The effect of the total solar eclipse of 29 March 2006 on meteorological variables in Greece, Atmos. Chem. Phys., 7, 5543–5553, doi:10.5194/acp-7-5543-2007, 2007.

Gerasopoulos, E., Zerefos, C. S., Tsagouri, I., Founda, D., Amiridis, V., Bais, A. F., Belehaki, A., Christou, N., Economou, G., Kanakidou, M., Karamanos, A., Petrakis, M., and Zanis, P.: The total solar eclipse of March 2006: overview, Atmos. Chem. Phys., 8, 5205–5220, doi:10.5194/acp-8-5205-2008, 2008.

Gogosheva, T. N., Petkov, B. K., and Krystev, D. G.: Measurement of ultraviolet radiation and ozone during the solar eclipse of August 11, 1999, Geomagn. Aeronomy, 42, 262–266, 2002.

Grell, G. A., Peckham, S. E., Schmitz, R., McKeen, S. A., Frost, G., Skamarock, W. C., and Eder, B.: Fully coupled "online" chemistry within the WRF model, Atmos. Environ., 39, 69576975, doi:10.1016/j.atmosenv.2005.04.027, 2005.

Hanna, E.: Meteorological effects of the solar eclipse of 11 August 1999, Weather, 55, 430–446, 2000.

Janjic, Z. I.: The step-mountain eta coordinate model: Further development of the convection, viscous sub-layer, and turbulent closure schemes, Mon. Weather Rev., 122, 927–945, 1994.

Kazadzis, S., Bais, A., Blumthaler, M., Webb, A., Kouremeti, N., Kift, R., Schallhart, B., and Kazantzidis, A.: Effects of total solar eclipse of 29 March 2006 on surface radiation, Atmos. Chem. Phys., 7, 5775–5783, doi:10.5194/acp-7-5775-2007, 2007.

Krishnan, P., Kunhikrishnan, P. K., Nair, S. M., Ravindran, S., Ramachandran, R., Subrahamanyam, D. B., and Ramana, M. V.: Observations of the atmospheric surface layer parameters over a semi arid region during the solar eclipse of August 11th, 1999, Proc. Indian Acad. Sci. (Earth Planet. Sci.), 113, 353–363, 2004.

Mims, F. M. and Mims, E. R.: Fluctuations in Column Ozone during the Total Solar Eclipse of July 11, 1991, Geophys. Res. Lett., 20, 367–370, 1993.

Mlawer, E. J., Taubman, S. J., Brown, P. D., Iacono, M. J., and Clough, S. A.: Radiative transfer for inhomogeneous atmospheres: RRTM, a validated correlated-k model for the longwave, J. Geophys. Res., 102, 16663–16682, 1997.

ACPD

11, 2473–2501, 2011

The effects of a solar eclipse on photo-oxidants in China

J.-B. Wu et al.

Psiloglou, B. E. and Kambezidis, H. D.: Performance of the meteorological radiation model during the solar eclipse of 29 March 2006, Atmos. Chem. Phys., 7, 6047–6059, doi:10.5194/acp-7-6047-2007, 2007.
Tzanis, C.: Ground-based observations of ozone at Athens, Greece during the solar eclipse of 1999, Int. J. Remote. Sens., 26, 3585–3596, doi:10.1080/01431160500076947, 2005.
Tzanis, C., Varotsos, C., and Viras, L.: Impacts of the solar eclipse of 29 March 2006 on the surface ozone concentration, the solar ultraviolet radiation and the meteorological parameters at Athens, Greece, Atmos. Chem. Phys., 8, 425–430, doi:10.5194/acp-8-425-2008, 2008.
Varotsos, C.: Solar Ultraviolet-Radiation and Total Ozone, as Derived from Satellite and Ground-Based Instrumentation, Geophys. Res. Lett., 21, 1787–1790, 1994.
Varotsos, C.: Airborne measurements of aerosol, ozone, and solar ultraviolet irradiance in the troposphere, J. Geophys. Res., 110, D09202, doi:10.1029/2004jd005397, 2005.
Wild, O., Zhu, X., and Prather, M. J.: Fast-j: Accurate simulation of in- and below-cloud photolysis in tropospheric chemical models, J. Atmos. Chem., 37, 245–282, 2000.
Zanis, P., Zerefos, C. S., Gilge, S., Melas, D., Balis, D., Ziomas, I., Gerasopoulos, E., Tzoumaka, P., Kaminski, U., and Fricke, W.: Comparison of measured and modeled surface ozone concentrations at two different sites in Europe during the solar eclipse on August 11, 1999, Atmos. Environ., 35, 4663–4673, 2001.
Zanis, P., Katragkou, E., Kanakidou, M., Psiloglou, B. E., Karathanasis, S., Vrekoussis, M., Gerasopoulos, E., Lisaridis, I., Markakis, K., Poupkou, A., Amiridis, V., Melas, D., Mihalopoulos, N., and Zerefos, C.: Effects on surface atmospheric photo-oxidants over Greece during the total solar eclipse event of 29 March 2006, Atmos. Chem. Phys., 7, 6061–6073, doi:10.5194/acp-7-6061-2007, 2007.
Zaveri, R. A. and Peters, L. K.: A new lumped structure photochemical mechanism for large-scale applications, J. Geophys. Res., 104, 30387–30415, 1999.
Zaveri, R. A., Easter, R. C., Fast, J. D., and Peters, L. K.: Model for Simulating Aerosol Interactions and Chemistry (MOSAIC), J. Geophys. Res., 113, D13204, doi:10.1029/2007jd008782, 2008.
Zerefos, C. S., Balis, D. S., Zanis, P., Meleti, C., Bais, A. F., Tourpali, K., Melas, D., Ziomas, I., Galani, E., Kourtidis, K., Papayannis, A., and Gogosheva, Z.: Changes in surface UV solar irradiance and ozone over the Balkans during the eclipse of August 11, 1999, Adv. Space Res., 27(12), 1955–1963, 2001.

ACPD
11, 2473–2501, 2011

Zerefos, C. S., Gerasopoulos, E., Tsagouri, I., Psiloglou, B. E., Belehaki, A., Herekakis, T., Bais, A., Kazadzis, S., Eleftheratos, C., Kalivitis, N., and Mihalopoulos, N.: Evidence of gravity waves into the atmosphere during the March 2006 total solar eclipse, Atmos. Chem. Phys., 7, 4943–4951, doi:10.5194/acp-7-4943-2007, 2007.

ACPD
11, 2473–2501, 2011

Table 1. Average differences of O_3, NO_2 and NO between Eclipse and NoEclipse conditions in WRF-Chem simulations over the time window of the eclipse 00:00–05:00 UTC. The values in parentheses correspond to the differences for the maximum sun coverage.

	ΔO_3 (ppbv)	ΔNO_2 (ppbv)	ΔNO (ppbv)	ΔCO (ppbv)
Polluted area	−5.15 (−7.03)	1.18 (3.17)	−0.23 (−1.54)	10.64 (13.07)
Clean area	−2.65 (−4.38)	0.47 (1.68)	−0.01 (−0.70)	2.46 (3.58)

ACPD
11, 2473–2501, 2011

Table 2. Average impacts (as a percentage, %) of the solar eclipse on photo-oxidants in the polluted and clean area respectively in different periods (according to solar obscuration for each domain: >50%, <50%, After eclipse(2 h)).". Values outside the brackets represent the impacts in the polluted area, and values inside the brackets represent the clean area. The impact of a solar eclipse is calculated using the formula: Percentage = (Eclipse – NoEclipse)/NoEclipse × 100%.

	Solar obscuration		
Species	> 50%	< 50%	After eclipse (2 h)
O_3	−24.8 (−17.3)	−14.0 (−8.2)	−6.0 (−2.0)
NO_2	51.9 (73.9)	37.1 (30.3)	28.4 (9.0)
NO	−48.3 (−88.3)	62.3 (47.6)	43.0 (11.9)
CO	10.3 (4.4)	8.0 (3.0)	3.9 (1.8)
OH	−73.7 (−79.9)	−16.1 (−3.57)	−0.2 (3.2)
HO_2	−54.8 (−63.6)	−35.2 (−16.2)	−16.7 (−2.5)
NO_3	28.3 (60.0)	−7.3 (−4.3)	−5.4 (−1.1)

ACPD
11, 2473–2501, 2011

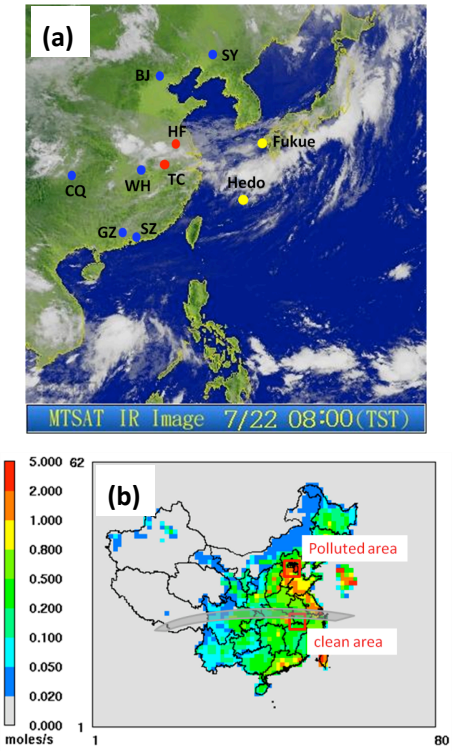

Fig. 1. **(a)** satellite image at the beginning of the solar eclipse (00:00 UTC, 22 July 2009, the blue points represent the observation sites with 2-m temperature data, the yellow points represent the observation sites with downward solar radiation data, the red points represent the observation sites with atmospheric pollutants data); **(b)** domain for WRF-Chem simulation with NO_2 emission (moles s^{-1}) from SMOKE model, the red box represents two areas with different emission levels, the shaded zone represents the path of the total solar eclipse across China. The domain-averaged maximum sun coverage is 74.1% in the polluted area and 96.8% in the clean area.

ACPD
11, 2473–2501, 2011

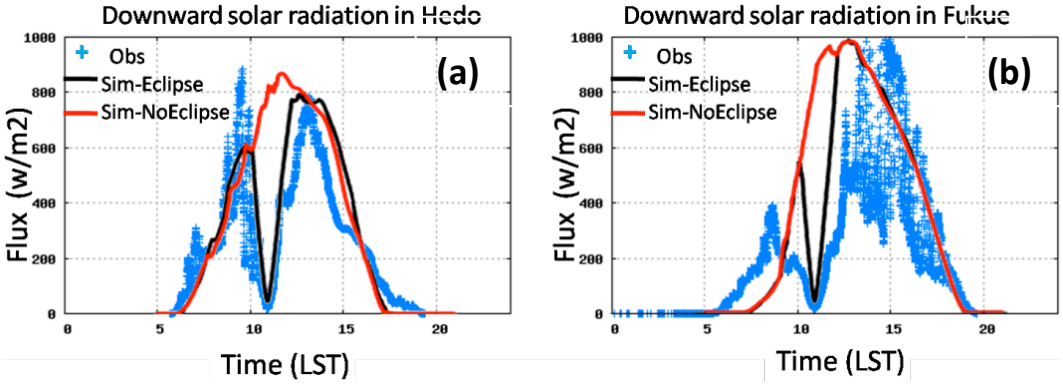

Fig. 2. Downward solar radiation flux (w m^{-2}) during the eclipse period at **(a)** Hedo (26.87 N, 128.25 E) and **(b)** Fukue (32.75 N, 128.68 E) which are showed as yellow points in Fig. 1a.

ACPD
11, 2473–2501, 2011

The effects of a solar eclipse on photo-oxidants in China

J.-B. Wu et al.

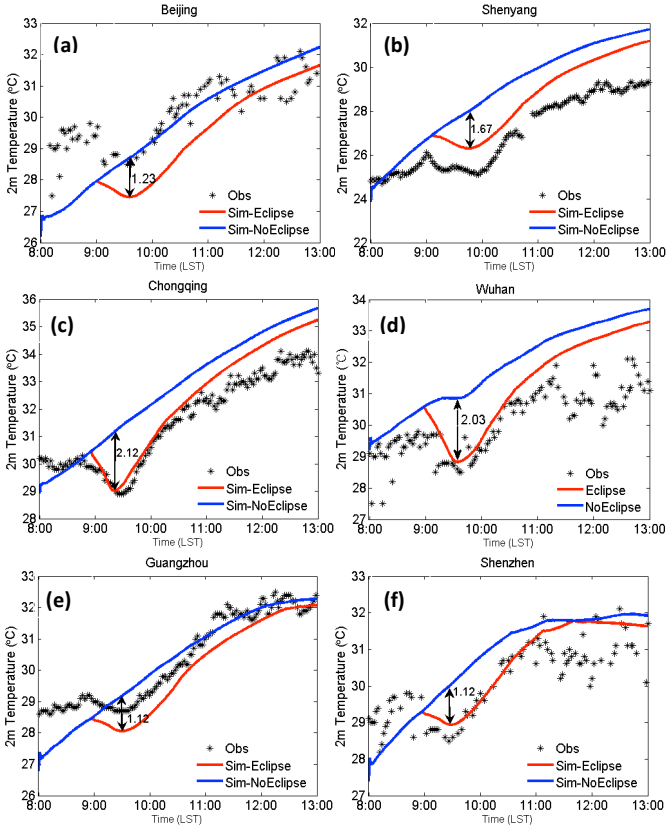

Fig. 3. Temporal variation of 2-m Temperature during the eclipse hours in the airports of **(a)** Beijing, **(b)** Shenyang, **(c)** Chongqing, **(d)** Wuhan, **(e)** Guangzhou, **(f)** Shenzhen. Double arrows denote the maximum difference in temperature between Eclipse and NoEclipse runs. The locations of each airport which are also depicted as blue points in Fig. 1a are: Beijing (BJ, 40.08 N, 116.61 E), Shenyang (SY, 41.64 N, 123.48 E), Chongqing (CQ, 29.72 N, 106,64 E), Wuhan (WH, 30.37 N, 114.20 E), Guangzhou (GZ, 23.39 N, 113.31 E), Shenzhen (SZ, 22.64 N, 113.80 E).

ACPD
11, 2473–2501, 2011

The effects of a solar eclipse on photo-oxidants in China

J.-B. Wu et al.

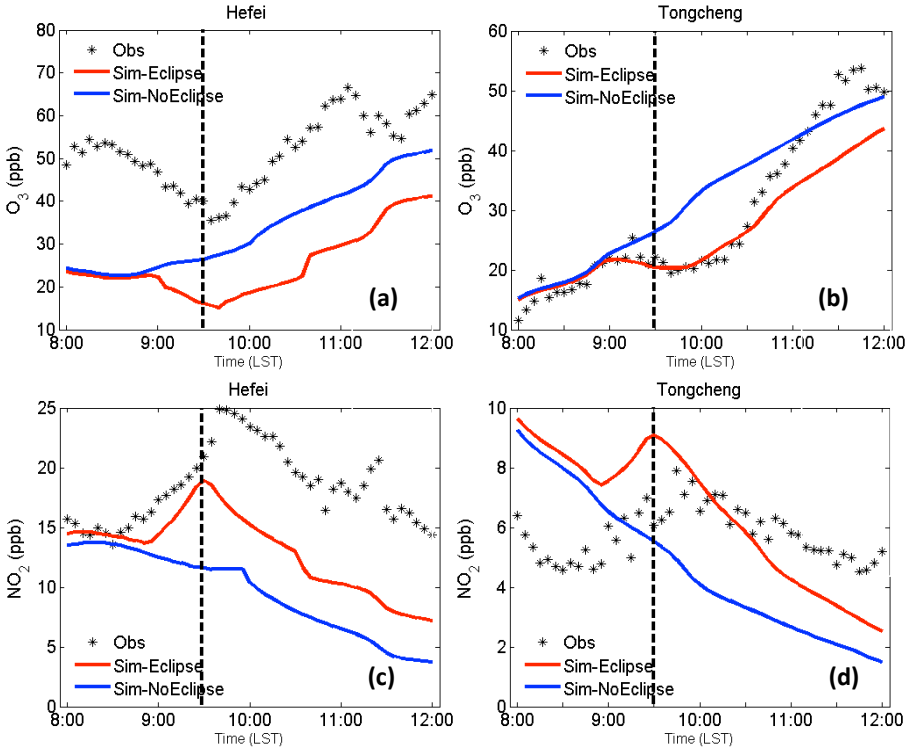

Fig. 4. Temporal variation of O_3 and NO_2 during the eclipse in Hefei **(a**, **c)** and Tongcheng **(b**, **d)**. The locations of these two sites which are also depicted as red points in Fig. 1a are: Hefei (HF, 31.51 N, 117.16 E) and Tongcheng (TC, 31.04 N, 116.94 E). The vertical dashed lines denote the maximum in the eclipse at each station.

ACPD
11, 2473–2501, 2011

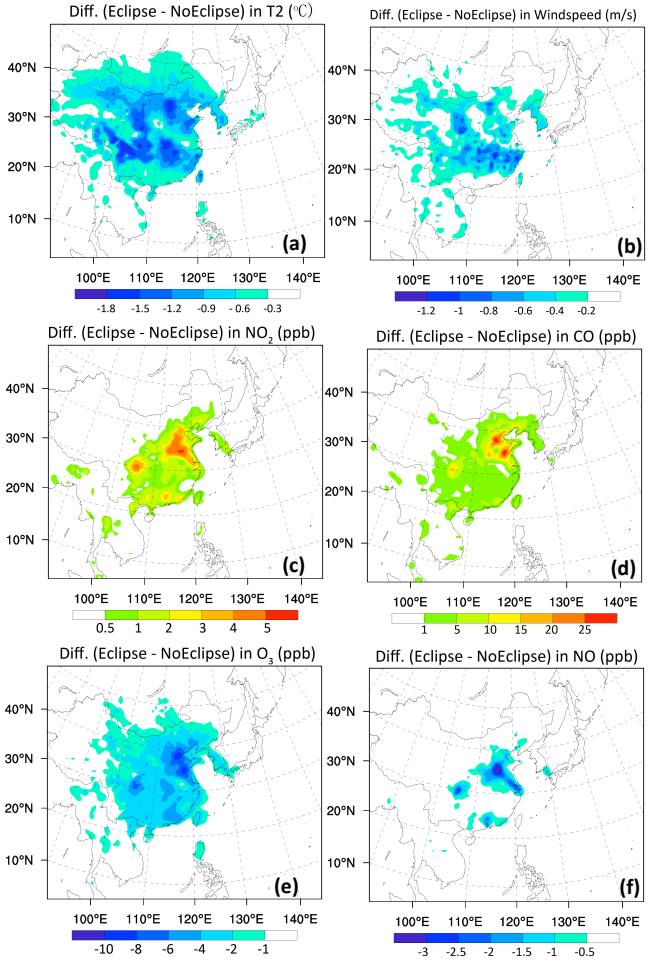

Fig. 5. Differences of **(a)** temperature, **(b)** windspeed, **(c)** NO_2, **(d)** CO, **(e)** O_3, **(f)** NO between Eclipse and NoEclipse conditions in the WRF-Chem simulations averaged over the time window of the eclipse 01:00–02:00 UTC.

ACPD
11, 2473–2501, 2011

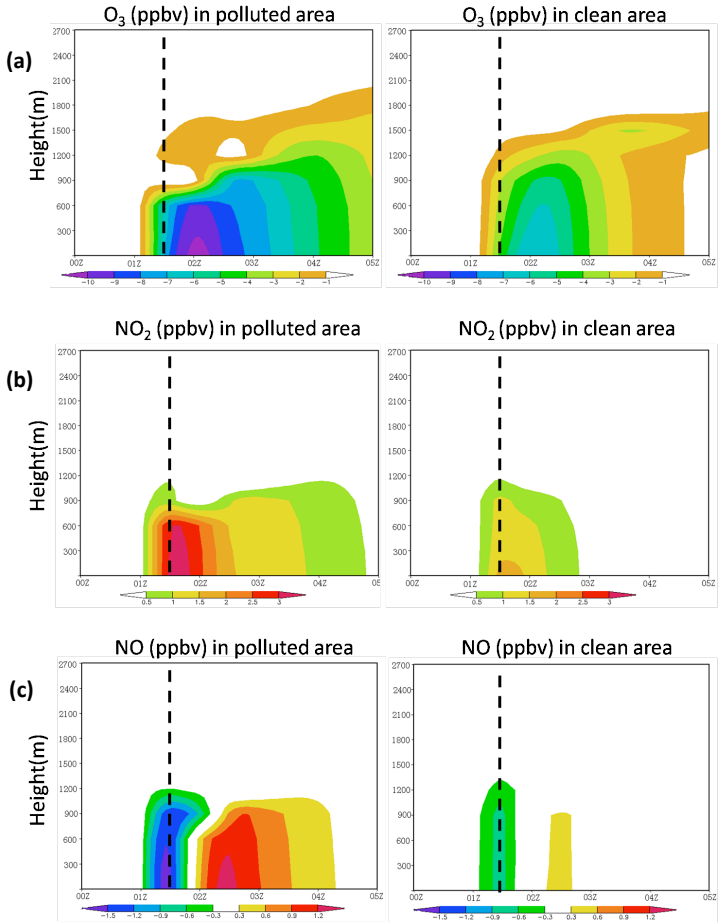

Fig. 6. The altitude-time cross sections of the differences between model simulations (Eclipse – NoEclipse) in **(a)** O_3, **(b)** NO_2, and **(c)** NO, domain-averaged over the polluted (left side) and clean (right side) areas. Dashed lines show the period of maximum solar eclipse in Beijing.

ACPD
11, 2473–2501, 2011

The effects of a solar eclipse on photo-oxidants in China

J.-B. Wu et al.

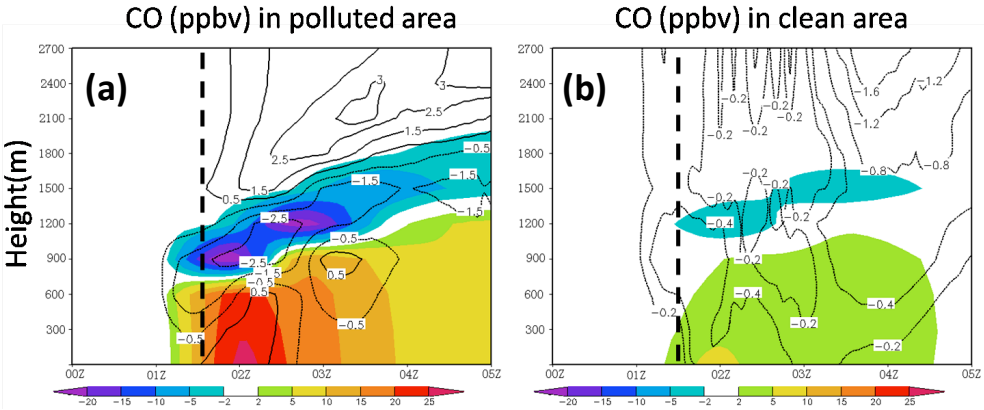

Fig. 7. Same as Fig. 6, but for CO in the polluted area **(a)** and in the clean area **(b)**. The contour represents the vertical wind velocity (10^{-3} m s^{-1}).

ACPD
11, 2473–2501, 2011

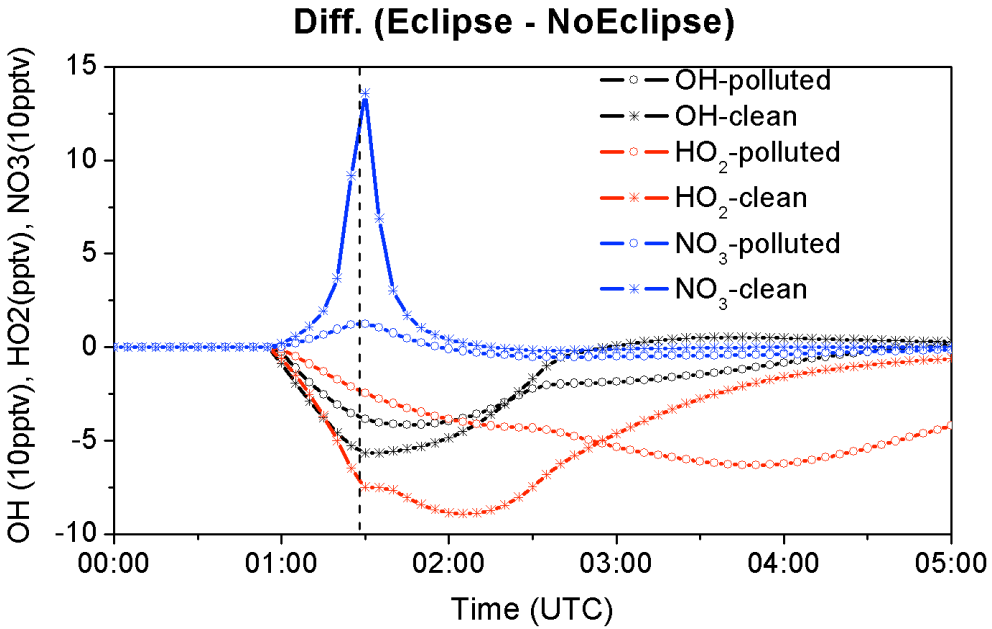

Fig. 8. Time series of differences in OH, HO_2, and NO_3 between Eclipse and NoEclipse runs. The dashed line shows the period of maximum solar eclipse in Beijing.

ACPD
11, 2473–2501, 2011